

Article

Macro-Scale Strength and Microstructure of ZrW_2O_8 Cementitious Composites with Tunable Low Thermal Expansion

Jianshu Ouyang ¹, Yangbo Li ^{2,*} , Bo Chen ² and Dahai Huang ¹

¹ School of Transportation Science and Engineering, Beihang University, Beijing 100191, China; auyeung@buaa.edu.cn (J.O.); huangdahai@buaa.edu.cn (D.H.)

² College of Hydraulic and Environmental Engineering, China Three Gorges University, Yichang 443002, China; 15672487483@163.com

* Correspondence: liyangbo@ctgu.edu.cn

Received: 11 April 2018; Accepted: 5 May 2018; Published: 7 May 2018



Abstract: Concretes with engineered thermal expansion coefficients, capable of avoiding failure or irreversible destruction of structures or devices, are important for civil engineering applications, such as dams, bridges, and buildings. In natural materials, thermal expansion usually cannot be easily regulated and an extremely low thermal expansion coefficient (TEC) is still uncommon. Here we propose a novel cementitious composite, doped with ZrW_2O_8 , showing a wide range of tunable thermal expansion coefficients, from $8.65 \times 10^{-6} \text{ }^\circ\text{C}^{-1}$ to $2.48 \times 10^{-6} \text{ }^\circ\text{C}^{-1}$. Macro-scale experiments are implemented to quantify the evolution of the thermal expansion coefficients, compressive and flexural strength over a wide range of temperature. Scanning Electron Microscope (SEM) imaging was conducted to quantify the specimens' microstructural characteristics including pores ratio and size. It is shown that the TEC of the proposed composites depends on the proportion of ZrW_2O_8 and the ambient curing temperature. Macro-scale experimental results and microstructures have a good agreement. The TEC and strength gradually decrease as ZrW_2O_8 increases from 0% to 20%, subsequently fluctuates until 60%. The findings reported here provide a new routine to design cementitious composites with tunable thermal expansion for a wide range of engineering applications.

Keywords: ZrW_2O_8 ; cementitious composites; low thermal expansion

1. Introduction

Cementitious Composites (CCs) are facile, economical structural materials, which are most widely applied in civil engineering [1]. But CCs have such innate shortcomings as brittleness, poor tensile strength, and poor thermal conductivity. In order to enhance structural integrity, researchers and engineers have usually focused on tuning their stiffness, strength, fracture toughness [2], self-healing capability [3,4], ductility [5,6], hydration [7,8] and shrinkage [9,10] through filling the cement matrix with micro-/nano- fibers [11], graphene [12,13], carbon nanotubes [14–17], silica fume [18,19], magnesium oxide (MgO) [20,21], plasticizer [22,23], hardening accelerator [24], and fly ash [25,26]. Among various loading conditions that often occur in concrete structures, the thermal load is a ubiquitous one, especially in massive concrete structures, causing thermal cracks or fractures, which are always the severest challenge for integrity and perfection of concrete structures. Thermal-induced cracks are often found in massive structures, for example, dams, bridges and buildings like China Three Gorges Dam, the Cathedral of Our Lady of the Angels in California, USA, and Odde-sund bridge in Denmark [1]. Until now, the problem of how to improve concrete's capability of resisting thermal load has not been effectively solved. Conventional approaches

include enhancing concrete's strength and lessening thermal stress. Enhancing concrete strength is implemented by increasing the quantity of cement per cubic meter, which usually accompanies increasing the Young's modulus of the concrete and hydration heat of the concrete and causes easier failure due to temperature amplitude. Lessening thermal stress is realized via controlling the initial temperature of concrete, hydration heat by low-heat substitution of cement, embedded cooling pipes and slicing unity into sections, which scarifies the unity of massive concrete structure and simultaneously results in higher costs and a longer construction process [27,28], since concrete is a poor conductor of heat. The application of 3D (three dimensional) printing technology in concrete fabrication [29–31], due to rapid prototyping, from fluidic to well-hydrated in a short time, without a mold, can lead to severer thermal stress and distortion in 3D-printed cementitious composites, analogous to the cementitious mortar.

According to classical thermo-mechanical theory, the upper limit of thermal stress is given as $\sigma = E\alpha\Delta T$, where E is the Young's Modulus, α the thermal expansion coefficient (TEC), and ΔT temperature increment. Therefore, reducing concrete's TEC is an alternative and soluble approach that might lessen thermal stress. Recently, many artificially synthesized materials with negative thermal expansion (NTE) spring up, for instance, Zirconium tungstate (ZrW_2O_8) and zirconium pyrovanadate (ZrV_2O_7) [32–35], which provide opportunities to decrease the TEC of synthesized composites. Metallic [36,37], metallic oxide [38,39], asphalt mastic [33] or polymeric [40] composites have realized the NTE effect by mixed with ZrW_2O_8 . Therefore, compared with conventional approaches, tuning TEC via doping with ZrW_2O_8 makes CCs insensitive to temperature variation to avoid cracks and ensure structural integrity without such side effects as extra elastic modulus increase, extra hydration heat, and extra costs. ZrW_2O_8 as filler in cement matrix was preliminarily explored in random synthesis [41]. But the feasibility of applying ZrW_2O_8 cementitious composites (ZCCs) in concrete is determined by their strength, stiffness, and toughness. Whether the NTE property of ZrW_2O_8 functions in the concrete structures' service environment is also rarely evaluated in prior research. Additionally, no one underscores the TEC of the concrete to lessen thermal stress.

Here, inspired by NTE synthesized composites, we present a new type of cementitious composite with tunable low thermal expansion, by mixing them with differently proportional ZrW_2O_8 . To assess their feasibility in engineering applications, the macro-scale thermo-mechanical experiments are performed to measure their TEC, compressive strength and flexural strength. The dependence of low thermal expansion and flexural and compressive strength on ZrW_2O_8 's percentage is also investigated by comparing the experimental results. Subsequently, the Scanning Electron Microscope (SEM) imaging is conducted to observe samples' microstructures including pore ratio and sizes, and to reveal the thermal deformation mechanism in the micro-scale. The feasibility and applicability of ZCCs in engineering applications are also discussed to ascertain the necessity of further researches on ZCCs.

2. Materials and Testing Methods

2.1. Materials

Standard cement mortars with 40 mm × 40 mm × 160 mm, mixed with different proportions of ZrW_2O_8 were made according to *Method of testing cement- Determination of strength* (GB-T 17671-1999) [42]. Experiments were conducted to test the coefficient of thermal expansion and the compressive and flexural strength. To explore ZrW_2O_8 's contribution to reducing the TEC of cementitious composites, seven groups of specimens were designed by the weight of ZrW_2O_8 with the weight ZrW_2O_8 /Cement Ratio (Z/C) = 0%, 10%, 20%, 30%, 40%, 50%, and 60%, whereas per group compromises three same specimens.

Ordinary Portland cement P.O42.5 (SanXia brand) used in this experiment as shown in Figure 1a consists of such chemical compositions as $3\text{CaO}\cdot\text{SiO}_2$ (C_3S), $2\text{CaO}\cdot\text{SiO}_2$ (C_2S), $3\text{CaO}\cdot\text{Al}_2\text{O}_3$ (C_3A) and $4\text{CaO}\cdot\text{Al}_2\text{O}_3\cdot\text{Fe}_2\text{O}_3$ (C_4AF), ranging 48%, 26%, 11%, and 16%, respectively. Chinese ISO standard sand is adopted, whose grain size ranges from 0.08 mm to 2 mm. ZrW_2O_8 , provided by Tiegao international

trade limited company of Shanghai as shown in Figure 1a, is a gray powder composed of angular particles typically in the size range from 4 μm to 7 μm . Drinking water is used to stir smooth.



Figure 1. Fabrication of cementitious composites including synthesis, molding, hydration, solidification, and maintenance. (a) ZrW_2O_8 and cement are the main ingredients of cementitious composites; (b) The stirrer is used to blend uniformly all the ingredients; (c) The vibrator is employed to exclude pores inside and densify composites; (d) Specimens are placed, hydrate and solidify in a water-bathing maintenance environment.

2.2. Fabrication of Specimens

Fabrication of specimens includes such main stages as synthesis, molding, hydration, solidification, and maintenance, as shown in Figure 1b–d. The composites consist of the cement, standard sand, water, and different proportions of ZrW_2O_8 as shown in Table 1. In the first stage, in order to evenly disperse ingredients, the synthesis has to obey the following procedures: the water, the cement and ZrW_2O_8 are poured first into the pot of the planet-like stirrer (Figure 1b) ready to be stirred for 30 s at a low speed. After that, standard sand is mixed into the composites with the high speed of stirring 30 s. Before completing the synthesis, the stirrer pauses for 90 s and then keeps going for 60 s. To avoid over-vibration or less-vibration of the mortar specimens, time deviation every step should be controlled less than one second.

Later, the composites are cast into 40 mm \times 40 mm \times 160 mm molds. To make specimens denser, the three linked molds with fluidic specimens should be vibrated on the specific machine as shown in Figure 1c. After totally compacted, the specimens are maintained in the constant temperature and moisture environment of 20 $^\circ\text{C}$ and 80%. This stage lasts for 24 h until specimens are removed from the molds. Eventually, they are placed in a water-bathing environment to hydrate and solidify for 28 days as shown in Figure 1d.

Table 1. Mix design.

No.	ZrW ₂ O ₈ /Cement (%)	Cement/(g)	Sand/(g)	Water/(mL)	ZrW ₂ O ₈ /(g)
1	0	450	1350	225	0
2	10	450	1350	225	45
3	20	450	1350	225	90
4	30	450	1350	225	135
5	40	450	1350	225	180
6	50	450	1350	225	225
7	60	450	1350	225	270

2.3. Testing

To clarify ZrW₂O₈'s role on the improvement of thermo-mechanical properties, the TEC, compressive strength, and flexural strength of differently proportional ZrW₂O₈ specimens was investigated in sequence. All the specimens experienced same maintaining and thermally and mechanically loading process. All the specimens' fabrication and the testing methods abide by *Method of testing cements-Determination of strength* (GB-T 17671-1999).

2.3.1. Testing the thermal expansion coefficient (TEC)

The TEC of specimens is measured by a strain meter (DH3815, Donghua Co., Ltd., Taizhou, China, Figure 2a) within a glass-window thermal oven with a controlled temperature as shown in Figure 2b. The temperature was gradually increased from room temperature (20 °C) to 120 °C and held for 30 min for each step to achieve a homogenous temperature distribution. Two strain gauges pasted by epoxy glue on literally opposite surfaces on the specific specimen are used to capture the thermal strains with the temperature increase. To ensure the strain gauges to represent the real thermal strain of specimens, we employ an extra constant strain gauge as the compensation, paste tightly two measured gauges connected to the strain meter, and take the average value of both. Before performing thermal load, we need to dry specimens more than 24 h and calibrate strain gauges. During the testing process, we read the strain value after calm indication on the meter.

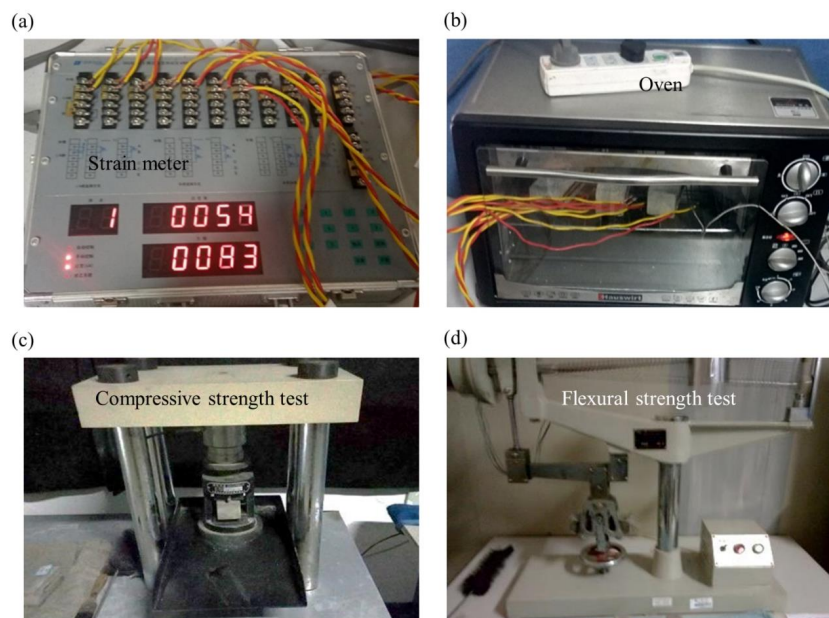


Figure 2. Experiments of thermal strain, compressive and flexural strength testing. (a) The strain meter aims to capture the thermal strain during the heating process; (b) The thermal load is realized by increasing the temperature in the oven; (c) The compressive testing machine; and (d) the flexural testing machine are applied to test the strength of specimens.

2.3.2. Flexural Strength Determination

The flexural strength is tested by double-lever electric testing machine (KZJ-5, Xidong CO., Ltd., Wuxi, China) as tri-point bending style as shown in Figure 2c. The machine loads as the velocity of 50 N/s on the specimen and records the force, F_f , at the moment the specimen is destroyed. The flexural strength is given by $[\sigma]_f = \frac{1.5F_f L}{b^3}$, where L is the distance between the supports, and b the width of cross section area.

2.3.3. Compressive Strength Testing

After flexural strength determination, every specimen is split into two halves, which are continuously used as samples to test the compressive strength on the testing machine (YAW-300, Zhongke Co., Ltd., Wuxi, China) as shown in Figure 2d. The machine loads at the velocity of 2.4 KN/s until the sample is destroyed.

2.4. Scanning Electron Microscope (SEM) Imaging

After performing macro-scale mechanical testing, the SEM imaging is conducted to observe specimens' pores ratio and size via SEM instrument (JSM-7500SEM, JEOL, Tokyo, Japan) and Analysis Software (Image Pro-Plus, Media Cybernetics, Inc., Rockville, MD, USA). We take some minor pieces of fragments from destroyed cross area on the specimens as imaging samples.

2.5. Theoretical Prediction of TEC

We adopt weighted average method in elastic modulus to prediction the TEC of ZCCs. The theoretical model is conducted as

$$\alpha = \frac{\alpha_p E_p V_p + \alpha_s E_s V_s + \alpha_g E_g V_g}{E_p V_p + E_s V_s + E_g V_g} \quad (1)$$

where $\alpha_p, \alpha_s, \alpha_g$ are the TECs of cement stone, sand and ZrW_2O_8 , respectively, and E_p, E_s, E_g the elastic modulus of cement stone, sand and ZrW_2O_8 , and V_p, V_s, V_g the volume fraction of cement stone, sand and ZrW_2O_8 . Here $V_p + V_s + V_g = 1$. The TEC of cement stone is $15\text{--}20 \times 10^{-6} \text{ }^\circ\text{C}^{-1}$, TEC of sand $12 \times 10^{-6} \text{ }^\circ\text{C}^{-1}$, and TEC of ZrW_2O_8 $-8.7 \times 10^{-6} \text{ }^\circ\text{C}^{-1}$.

3. Results and Discussion

3.1. Macro-Thermo-Mechanical Properties

Figure 3 reports the changes of thermal strains with the increase of temperature from room temperature ($20 \text{ }^\circ\text{C}$) to $120 \text{ }^\circ\text{C}$ among different proportional ZrW_2O_8 cementitious composite specimens. Figure 4 shows the evolutions of TEC, flexural strength, compressive strength and compression/flexure ratio with the increase of ZrW_2O_8 . The standard cement mortar's compressive strength at 28 d age is 28 MPa, flexural strength is 7.8 MPa, which indicates that the experiments are reliable. According to theoretical prediction mentioned above, we calculated the TEC of 0% ZCC, $\alpha_{0\%} = 8.93 \times 10^{-6} \text{ }^\circ\text{C}^{-1}$, and the TEC of 30% ZCC $\alpha_{30\%} = 4.08 \times 10^{-6} \text{ }^\circ\text{C}^{-1}$, which is close to the experimental results and further verifies the reliability of our experiments.

Comparing thermal strains in Figure 3a–i, we observe that in general, as the proportion of ZrW_2O_8 increases, the maximum thermal strain gradually falls from approximately 800 to 300×10^{-6} , which is 62.5% of non- ZrW_2O_8 CCs. But, at a relatively low level of temperature increment, less than $80 \text{ }^\circ\text{C}$, thermal responses of all ZrW_2O_8 cementitious composites remain steady. When temperature moderately rises to $80 \text{ }^\circ\text{C}$ or higher, the thermal strains of all the specimens climb considerably high values, which vary with the percentage of ZrW_2O_8 . It manifests that sand and ZrW_2O_8 play the same roles in influencing the TEC of the composite when the ambient temperature is less than $80 \text{ }^\circ\text{C}$. After that, when ambient temperature is larger than $80 \text{ }^\circ\text{C}$, the negative thermal expansion (NTE) property of ZrW_2O_8 takes effect, pulling back

positive thermal expansion from the sand. Hence, the TEC of ZCCs is a function of ambient temperature rather than a constant value. In overall, the TEC of ZCCs reduces 65% with ZrW_2O_8 increase, compared with non- ZrW_2O_8 CCs. However, in civil engineering applications, such as dams, bridges, buildings and so on, most service environments or thermal loads are lower than $80\text{ }^\circ\text{C}$, which indicates that ZCC is a possible candidate for reducing thermal stress or distortion.

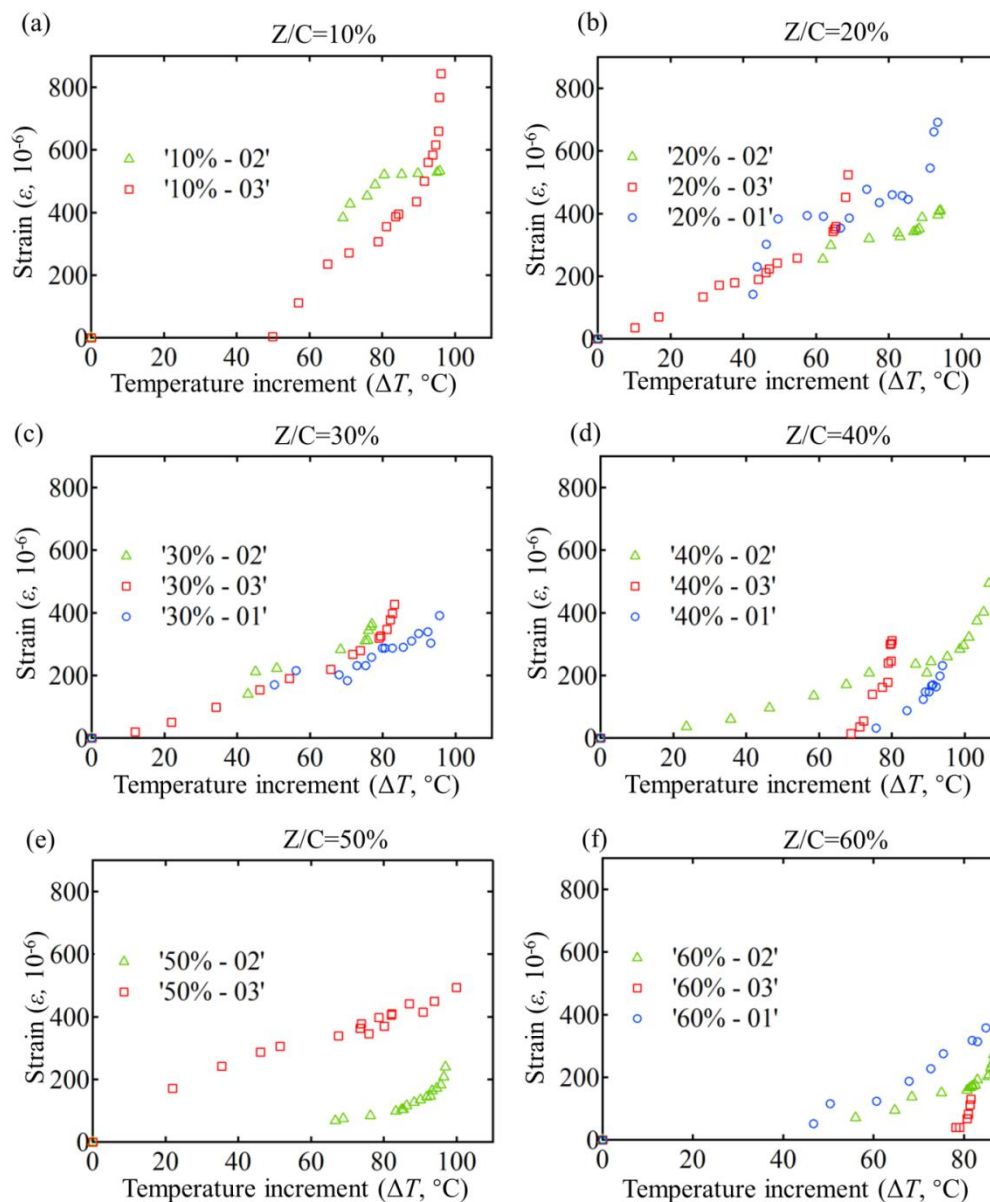


Figure 3. The thermal response of different proportional ZrW_2O_8 cementitious composites specimens with $Z/C =$ (a) 10%, (b) 20%, (c) 30%, (d) 40%, (e) 50%, and (f) 60%. (The titles in the legends in Figure 3 mean “ ZrW_2O_8 /Cement in weight—the number of the specimens with the same mix design”).

Furthermore, the strength of the NTE materials is crucial for potential applications. To study the mechanical properties, especially the strength of the proposed composites, uniaxial compression and 3-point flexure are carried out according to the standard testing method. The evolution of TECs, flexural and compressive strength, as well as compression/flexure ratio with ZrW_2O_8 's proportion increase in Figure 4, show that the TEC and strength gradually decrease as ZrW_2O_8 increases from 0% to 20%, and subsequently fluctuates until 60%. ZrW_2O_8 used in our experiment is a gray powder

composed of angular particles typically in the size range from 4 to 7 μm , while Chinese ISO standard sand adopted ranges from 80 μm to 2000 μm in grain size. Mixture of sand and cement causes capillary cavities or voids between grains and cement particles. And ZrW_2O_8 powder will likely fill capillary cavities or voids when it is doped. That is why the ratios and sizes of porosities decrease with increase of ZrW_2O_8 . In general, the strength of cement mortar decreases with the increase of percentage of small-size particles, because small particles cause weaker binding in hydrated mixtures.

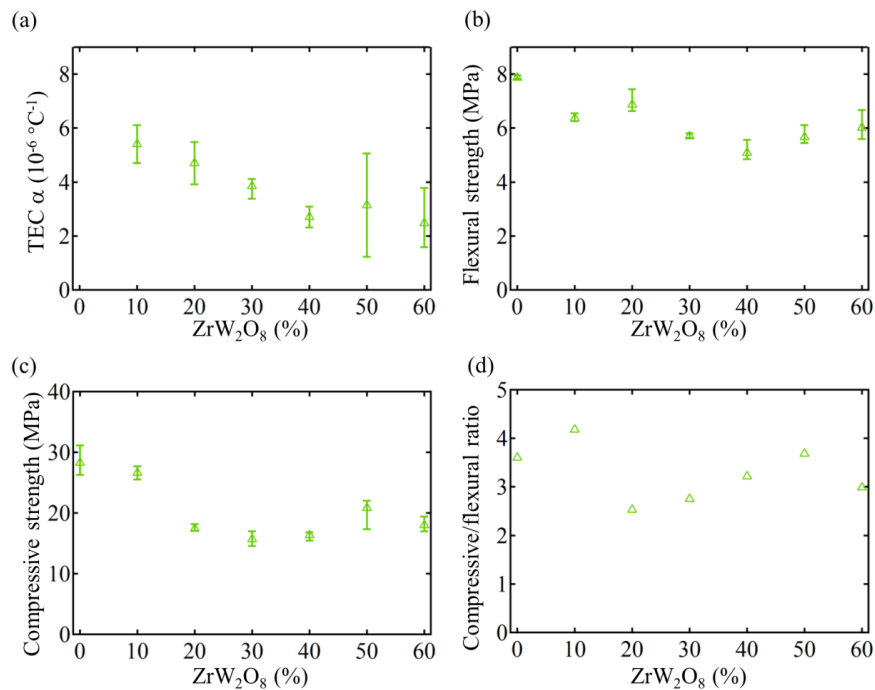


Figure 4. The change of (a) thermal expansion coefficient (TEC), (b) flexural strength, (c) compressive strength and (d) compression/flexure ratio with the increase of ZrW_2O_8 proportions.

3.2. SEM Analysis

In order to validate further macro-scale thermo-mechanical properties of ZCCs, the SEM imaging is conducted to amplify 500 times the surface of fragments of specimens, which is produced from flexural testing. SEM images of ZCCs of different percentages from 0% to 60% are listed in Figure 5a–g.

Comparison on ratios and sizes of pores imaged in those specimens as shown in Figure 5a–h implies that the greater the proportion of ZrW_2O_8 is, the lower the porous rate and size are. In regard to grain diameter of aggregates, the ISO sand is within 80–2000 μm , while ZrW_2O_8 is 4–7 μm . This is why 4–12 μm porous holes scatter in the section of pure cementitious composites, while fewer and smaller capillary voids occur in ZCCs regardless of the proportions. Actually, the ZrW_2O_8 , as a type of filler, fills in the gaps of sand aggregates. When thermal load is exerted on the ZCCs or pure cementitious composite, ZrW_2O_8 's negative thermal expansion takes effect by virtue of C–S–H binding. Therefore, the existence of ZrW_2O_8 induces in ZCCs the reduction of the thermal expansion coefficient, however, as the proportion of ZrW_2O_8 rises, the TEC does not continuously decrease but fluctuates especially at 40%–60%. As for compressive and flexural strength, because ZrW_2O_8 only fills in 4–12 μm pore holes (nevertheless, loads are usually borne by more than 80 μm bonded sand aggregates), the mixed ZrW_2O_8 does not sharply shorten ZCCs' strength, but keep stable on a 60%–70% strength of pure cementitious composite as the proportion increase until 60%. In a word, microstructures of ZCCs further confirm rationality of macro-scale mechanical testing.

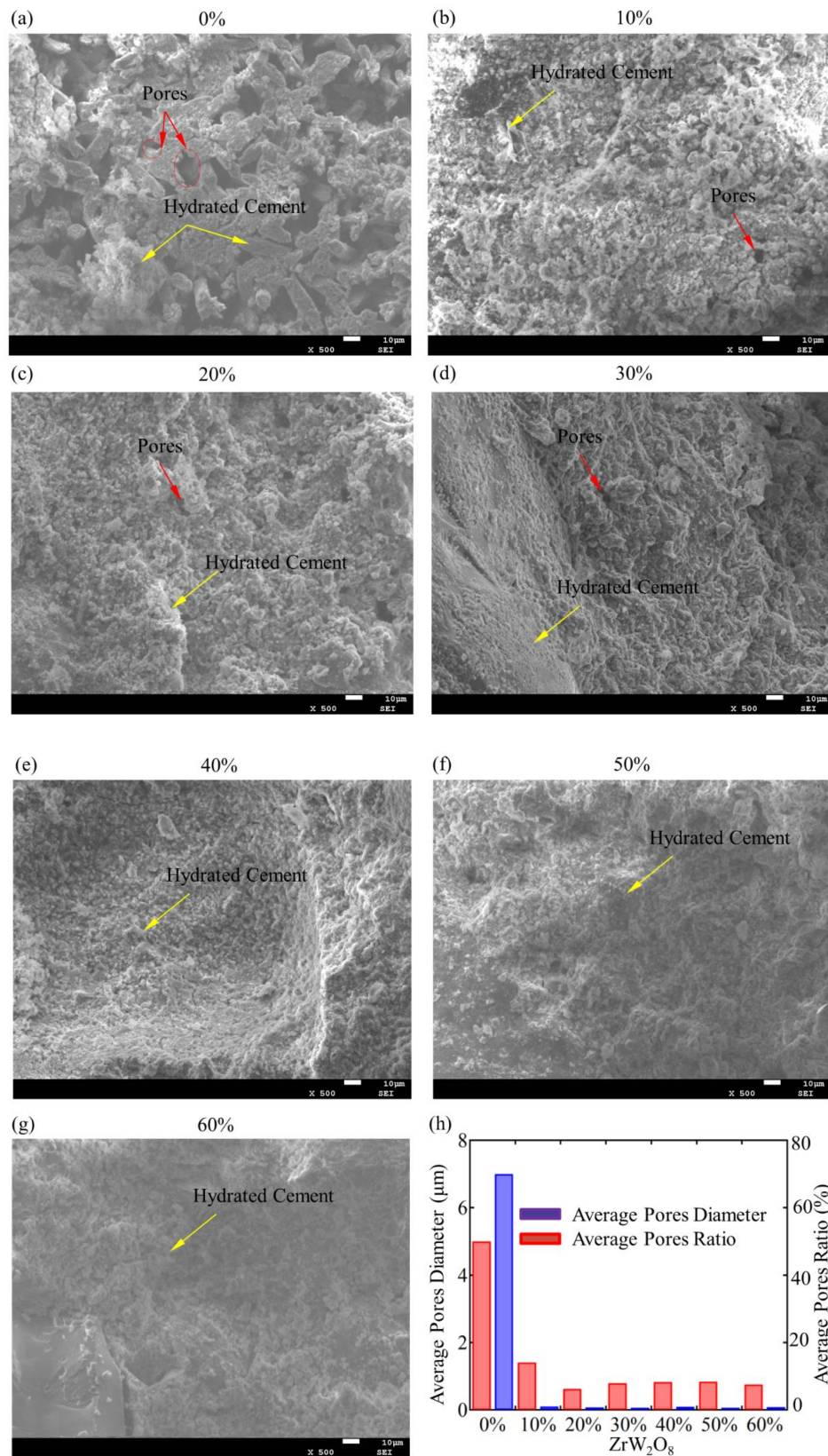


Figure 5. Scanning Electron Microscope (SEM) images of ZrW₂O₈ cementitious composites (ZCCs) of such percentages as 0% (a), 10% (b), 20% (c), 30% (d), 40% (e), 50% (f) and 60% (g), the size and ratio of the porosity of the ZCCs specimens in the SEM images (h). The ratios and sizes of porosities among those specimens decrease with the increase of ZrW₂O₈'s proportions.

4. Conclusions

In summary, to achieve cementitious composites insensitive to temperature variation, in order to avoid cracks and ensure structural integrity without such side effects as extra elastic modulus increase, extra hydration heat, and extra costs, we have demonstrated an approach to create ZrW_2O_8 cementitious composites with tunable thermal expansion coefficient ranging from $8.65 \times 10^{-6} \text{ }^\circ\text{C}^{-1}$ to $2.48 \times 10^{-6} \text{ }^\circ\text{C}^{-1}$. Through systematic macro-scale experiments on thermal expansion coefficient, compressive strength, and flexural strength, we have shown simultaneously that the thermal expansion coefficient of the cementitious composites can be tuned by varying the percentage of ZrW_2O_8 and the cementitious composites possess the effective strength to endure considerable loads. In particular, negative thermal expansion property of ZrW_2O_8 only plays a vital role on compensating the positive thermal expansion when the ambient temperature is more than $80 \text{ }^\circ\text{C}$. SEM imaging indicates that approximate $10 \text{ }\mu\text{m}$ pores scatter in pure cementitious composites (0%), while fewer occur in 10–60% ZCCs, which further verify the macro-scale mechanical experimental results. The results presented here not only demonstrate the development of a new type of engineering cementitious composites with tunable thermal expansion but also offer a wide range of potential applications in civil engineering structures, where thermal stress induced cracks are of great concern in structural design. The findings provide us opportunities to extend the studies on ZCCs with longer curing ages, and from cementitious mortar (without coarse aggregate) on the small specimens to the concrete on the large specimens, to see how the materials developed can reduce thermal stress and maintain the structural integrity under extreme environmental conditions or 3D printing processes. Future work will be directed toward the real-world engineering applications of the newly developed cementitious composites. Importantly, for the measurement of TEC and thermal field in engineering structures, we will use the distributed optical fiber sensor system. In addition, finite element-based computational models will be developed to predict the temperature field and thermal stress field. Collectively, the testing and computational modeling will provide us a better understanding on the effectiveness of the new developed cementitious composites in various engineering applications.

Author Contributions: Y.L. and D.H. conceived and designed the experiments; B.C. performed the experiments; J.O. and Y.L. analyzed the data; Y.L. contributed reagents/materials/analysis tools; Y.L. wrote the paper.

Funding: Y. Li gratefully acknowledges the financial support from the China Scholarship Council (File No. 201508420188).

Acknowledgments: The authors acknowledge Qianping reservoir concrete engineering projects (Grant No. QPSK-KY-07).

Conflicts of Interest: The authors declare no conflict of interest.

Nomenclature and Acronym

ZrW_2O_8	Zirconium tungstate
TEC	Thermal expansion coefficient
SEM	Scanning Electron Microscope
CCs	Cementitious Composites
MgO	Magnesium oxide
3D	Three dimensional
σ	Thermal stress
E	Young's Modulus
α	TEC (Thermal expansion coefficient)
ΔT	Temperature increment
NTE	Negative thermal expansion
ZrV_2O_7	Zirconium pyrovanadate
ZCCs	ZrW_2O_8 cementitious composites
Z/C	ZrW_2O_8 /Cement Ratio
F_f	Force while the specimen is destroyed in the flexural test
$[\sigma]_f$	Flexural strength
L	Distance between the supports in three-point flexural test
b	Width of cross section area.
$\alpha_p, \alpha_s, \alpha_g$	TECs of cement stone, sand and ZrW_2O_8 , respectively
E_p, E_s, E_g	Elastic modulus of cement stone, sand and ZrW_2O_8
V_p, V_s, V_g	Volume fraction of cement stone, sand and ZrW_2O_8

References

1. Kumar Mehta, P.; Monteiro, P.J.M. *Concrete Microstructure, Properties, and Materials*; McGraw-Hill: New York, NY, USA, 2006.
2. Hu, Y.; Luo, D.; Li, P.; Li, Q.; Sun, G. Fracture toughness enhancement of cement paste with multi-walled carbon nanotubes. *Constr. Build. Mater.* **2014**, *70*, 332–338. [[CrossRef](#)]
3. Luo, J.; Chen, X.; Crump, J.; Zhou, H.; Davies, D.G.; Zhou, G.; Zhang, N.; Jin, C. Interactions of fungi with concrete: Significant importance for bio-based self-healing concrete. *Constr. Build. Mater.* **2018**, *164*, 275–285. [[CrossRef](#)]
4. Granger, S.; Loukili, A.; Pijaudier-Cabot, G.; Chanvillard, G. Experimental characterization of the self-healing of cracks in an ultra high performance cementitious material: Mechanical tests and acoustic emission analysis. *Cem. Concr. Res.* **2007**, *37*, 519–527. [[CrossRef](#)]
5. Lee, J.M.; Lee, Y.J.; Jung, Y.J.; Park, J.H.; Lee, B.S.; Kim, K.H. Ductile capacity of reinforced concrete columns with electric arc furnace oxidizing slag aggregate. *Constr. Build. Mater.* **2018**, *162*, 781–793. [[CrossRef](#)]
6. Rakgate, S.M.; Dundu, M. Strength and ductility of simple supported R/C beams retrofitted with steel plates of different width-to-thickness ratios. *Eng. Struct.* **2018**, *157*, 192–202. [[CrossRef](#)]
7. Wild, S.; Khatib, J.M.; Jones, A. Relative strength, pozzolanic activity and cement hydration in superplasticised metakaolin concrete. *Cem. Concr. Res.* **1996**, *26*, 1537–1544. [[CrossRef](#)]
8. Berry, E.E.; Hemmings, R.T.; Zhang, M.H.; Cornelius, B.J.; Golden, M.D. Hydration in high-volume fly ash concrete binders. *ACI Mater. J.* **1994**, *91*, 382–389.
9. Shah, S.P.; Karaguler, M.E.; Sarigaphuti, M. Effects of shrinkage-reducing admixtures on restrained shrinkage cracking of concrete. *ACI Mater. J.* **1992**, *89*, 289–295.
10. Chen, P.W.; Chung, D.D.L. Low-drying-shrinkage concrete containing carbon fibers. *Compos. Part B Eng.* **1996**, *27*, 269–274. [[CrossRef](#)]
11. Chuah, S.; Pan, Z.; Sanjayan, J.G.; Wang, C.M.; Duan, W.H. Nano reinforced cement and concrete composites and new perspective from graphene oxide. *Constr. Build. Mater.* **2014**, *73*, 113–124. [[CrossRef](#)]
12. Pan, Z.; He, L.; Qiu, L.; Korayem, A.H.; Li, G.; Zhu, J.W.; Collins, F.; Li, D.; Duan, W.H.; Wang, M.C. Mechanical properties and microstructure of a graphene oxide–cement composite. *Cem. Concr. Compos.* **2015**, *58*, 140–147. [[CrossRef](#)]
13. Gong, K.; Pan, Z.; Korayem, A.H.; Qiu, L.; Li, D.; Collins, F.; Wang, C.M.; Duan, W.H. Reinforcing Effects of Graphene Oxide on Portland Cement Paste. *J. Mater. Civ. Eng.* **2015**, *27*, 1–6. [[CrossRef](#)]
14. Chan, L.Y.; Andrawes, B. Finite element analysis of carbon nanotube/cement composite with degraded bond strength. *Comput. Mater. Sci.* **2010**, *47*, 994–1004. [[CrossRef](#)]
15. Saafi, M.; Andrew, K.; Tang, P.L.; McGhon, D.; Taylor, S.; Rahman, M.; Yang, S.; Zhou, X. Multifunctional properties of carbon nanotube/fly ash geopolymeric nanocomposites. *Constr. Build. Mater.* **2013**, *49*, 46–55. [[CrossRef](#)]
16. Xu, S.; Liu, J.; Li, Q. Mechanical properties and microstructure of multi-walled carbon nanotube-reinforced cement paste. *Constr. Build. Mater.* **2015**, *76*, 16–23. [[CrossRef](#)]
17. Wang, B.; Han, Y.; Liu, S. Effect of highly dispersed carbon nanotubes on the flexural toughness of cement-based composites. *Constr. Build. Mater.* **2013**, *46*, 8–12. [[CrossRef](#)]
18. Kim, H.K.; Nam, I.W.; Lee, H.K. Enhanced effect of carbon nanotube on mechanical and electrical properties of cement composites by incorporation of silica fume. *Compos. Struct.* **2014**, *107*, 60–69. [[CrossRef](#)]
19. Stynoski, P.; Mondal, P.; Marsh, C. Effects of silica additives on fracture properties of carbon nanotube and carbon fiber reinforced Portland cement mortar. *Cem. Concr. Compos.* **2015**, *55*, 232–240. [[CrossRef](#)]
20. Zhang, R.; Panesar, D.K. New approach to calculate water film thickness and the correlation to the rheology of mortar and concrete containing reactive MgO. *Constr. Build. Mater.* **2017**, *150*, 892–902. [[CrossRef](#)]
21. Altun, İ.A.; Yilmaz, İ. Study on steel furnace slags with high MgO as additive in Portland cement. *Cem. Concr. Res.* **2002**, *32*, 1247–1249. [[CrossRef](#)]
22. Mendoza, O.; Sierra, G.; Tobón, J.I. Influence of super plasticizer and Ca(OH)₂ on the stability of functionalized multi-walled carbon nanotubes dispersions for cement composites applications. *Constr. Build. Mater.* **2013**, *47*, 771–778. [[CrossRef](#)]
23. Kamoun, A.; Jelidi, A.; Chaabouni, M. Evaluation of the performance of sulfonated esparto grass lignin as a plasticizer–water reducer for cement. *Cem. Concr. Res.* **2003**, *33*, 995–1003. [[CrossRef](#)]

24. Pan, W.; Ding, Z.; Chen, Y. Effects of TEA·HCl hardening accelerator on the workability of cement-based materials. *Mater. Sci. Eng. Conf. Ser.* **2017**, *182*, 012046. [[CrossRef](#)]
25. Langan, B.W.; Weng, K.; Ward, M.A. Effect of silica fume and fly ash on heat of hydration of Portland cement. *Cem. Concr. Res.* **2002**, *32*, 1045–1051. [[CrossRef](#)]
26. Diamond, S. Effects of two Danish flyashes on alkali contents of pore solutions of cement-flyash pastes. *Cem. Concr. Res.* **1981**, *11*, 383–394. [[CrossRef](#)]
27. Yangbo, L.; Dahai, H.; Jiashu, O. Fast algorithms of the simulation analysis of the thermal stresses on concrete dams during construction periods. *Phys. Procedia* **2012**, *24*, 1171–1177. [[CrossRef](#)]
28. Zhu, B. *Thermal Stress and Temperature Control in Massive Concrete*; Power Publisher of China: Beijing, China, 1999.
29. Paul, S.C.; Yi, W.D.T.; Panda, B.; Ming, J.T. Fresh and hardened properties of 3D printable cementitious materials for building and construction. *Arch. Civ. Mech. Eng.* **2018**, *18*, 311–319. [[CrossRef](#)]
30. Sanjayan, J.G.; Nematollahi, B.; Xia, M.; Marchment, T. Effect of surface moisture on inter-layer strength of 3D printed concrete. *Constr. Build. Mater.* **2018**, *172*, 468–475. [[CrossRef](#)]
31. Asprone, D.; Auricchio, F.; Menna, C.; Mercuri, V. 3D printing of reinforced concrete elements: Technology and design approach. *Constr. Build. Mater.* **2018**, *165*, 218–231. [[CrossRef](#)]
32. Pryde, A.K.A.; Hammonds, K.D.; Dove, M.T.; Heine, V.; Gale, J.D.; Warren, M.C. Origin of the negative thermal expansion in ZrW_2O_8 and ZrV_2O_7 . *J. Phys. Condens. Matter* **1996**, *8*, 10973–10982. [[CrossRef](#)]
33. Yi, J.; Cao, Y.; Feng, D.; Huang, Y. Characterization of zirconium tungstate filler and performance investigation on asphalt mastic made with zirconium tungstate filler. *Constr. Build. Mater.* **2016**, *125*, 387–397. [[CrossRef](#)]
34. Neely, L.A.; Kochergin, V.; See, E.M.; Robinson, H.D. Negative thermal expansion in a zirconium tungstate/epoxy composite at low temperatures. *J. Mater. Sci.* **2014**, *49*, 392–396. [[CrossRef](#)]
35. Duan, N.U.; Kameswari, A.; Sleight, A.W. Further Contraction of ZrW_2O_8 . *J. Am. Chem. Soc.* **2013**, *121*, 10432–10433. [[CrossRef](#)]
36. Sheng, J.; Wang, L.D.; Li, D.; Cao, W.P.; Feng, Y.; Wang, M.; Yang, Z.Y.; Zhao, Y.; Fei, W.D. Thermal expansion behavior of copper matrix composite containing negative thermal expansion $PbTiO_3$ particles. *Mater. Des.* **2017**, *132*, 442–447. [[CrossRef](#)]
37. Peng, Z.; Sun, Y.Z.; Peng, L.M. Hydrothermal synthesis of ZrW_2O_8 nanorods and its application in ZrW_2O_8 /Cu composites with controllable thermal expansion coefficients. *Mater. Des.* **2014**, *54*, 989–994. [[CrossRef](#)]
38. Yang, X.; Cheng, X.; Yan, X.; Yang, J.; Fu, T.; Qiu, J. Synthesis of ZrO_2 / ZrW_2O_8 composites with low thermal expansion. *Compos. Sci. Technol.* **2007**, *67*, 1167–1171. [[CrossRef](#)]
39. Sun, L.; Kwon, P. ZrW_2O_8 / ZrO_2 composites by in situ synthesis of $ZrO_2 + WO_3$: Processing, coefficient of thermal expansion, and theoretical model prediction. *Mater. Sci. Eng. A* **2009**, *527*, 93–97. [[CrossRef](#)]
40. Lin, K.; Qiu, S.; Lin, B.; Wang, Y. An Investigation of the Thermal Expansion Coefficient for Resin Concrete with ZrW_2O_8 . *Appl. Sci.* **2015**, *5*, 367–379. [[CrossRef](#)]
41. Kofteros, M.; Rodriguez, S.; Tandon, V.; Murr, L.E. A preliminary study of thermal expansion compensation in cement by ZrW_2O_8 additions. *Scr. Mater.* **2001**, *45*, 369–374. [[CrossRef](#)]
42. Chinese Building Materials Academy. *Method of Testing Cement-Determination of Strength*; China Standards Press: Beijing, China, 1999.

